Supporting Information

Chemically assembled anion exchange membrane surface for monovalent anion selectivity and fouling reduction

Yan Zhao, [a] Yi Li, [a] Shushan Yuan, [a] Junyong Zhu, [a] Sofie Houtmeyers, [a] Jian Li, [a] Raf Dewil, [a] Congjie Gao, [b] and Bart Van der Bruggen *[a, c]

[a]Department of Chemical Engineering, KU Leuven, Celestijnenlaan 200F, B-3001 Leuven, Belgium

[b]Center for Membrane Separation and Water Science & Technology, Ocean College, Zhejiang University of Technology, Hangzhou 310014, P. R. China

[c]Faculty of Engineering and the Built Environment, Tshwane University of Technology, Private Bag X680, Pretoria 0001, South Africa

*Corresponding author.

.

Corresponding Author: bart.vanderbruggen@kuleuven.be

This PDF file includes:

Texts S1 to S3

Figure S1 to Figure S13

Table S1 to S5

References (20)

Contents

1. Theories

1.1. The main theory for anion exchange membranes with selective separation of monovalent anions.

The three main aspects for preparation of AEMs with selective separation of monovalent anions:

1) The fixed ion exchange sites and the solution counter ions electrostatic repulsion forces effect, see in Figure S1;

2) The hydrated ionic diameter of different anions and AEMs structure sieving effect, see in Figure S2;

3) The mobility of anions cross the AEMs, see in Figure S3.

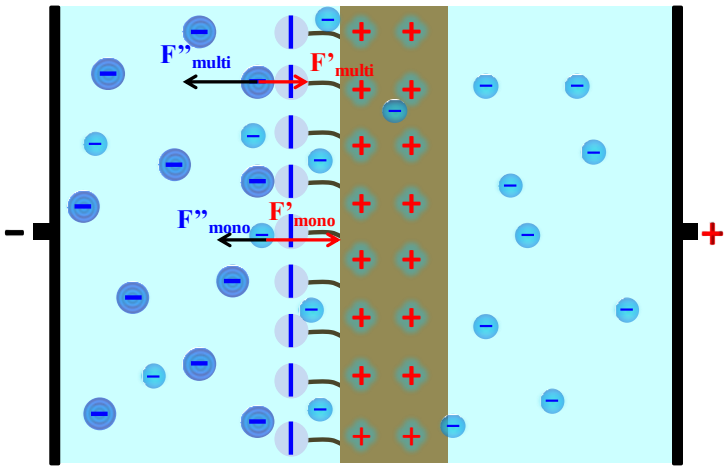

F=F'-F''
If F > 0, anions through the membrane;
If F < 0, anions will not through the membrane.

Figure S1. The electrostatic repulsion forces effect for selective separation of monovalent anions. Due to the F (monovalent) > 0, monovalent anions will through; while, for multivalent anions, F (multivalent) < 0, these kinds of anions will not through the membrane.

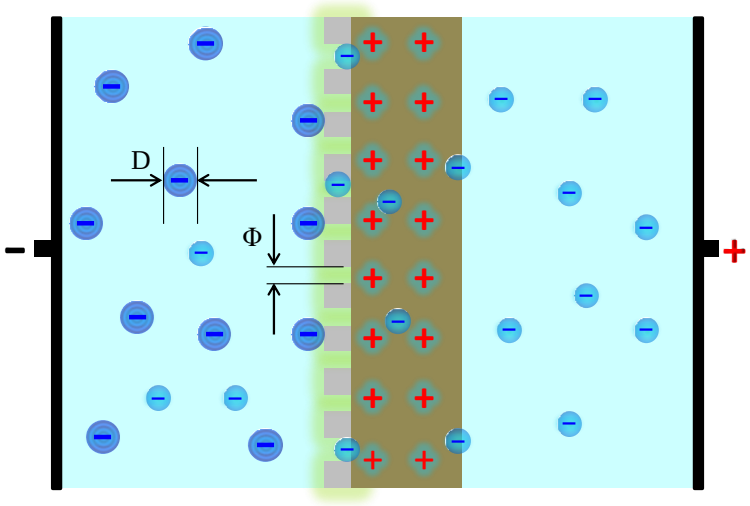

If Φ > D, anions through the membrane;
If Φ < D, anions will not through the membrane.

Figure S2. The sieving effect. If the hydrated ion diameter (In practice, the totally ionic hydration energy, hydrogen bond energy and each of the hydrogen bond energy and electric field force will contribute the resulting hydrated ion diameter) < membrane pore size, the anion will through; otherwise, the anion will not through the membrane.

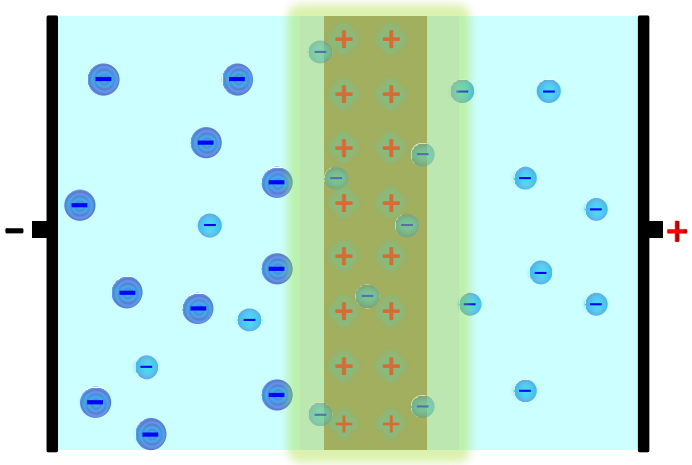

The selective separation of anions may effect by the binding affinity to the fixed ion exchange sites, pH, specific ion channel, est..

Figure S3. The mobility of ions cross the membrane effect. There are many reasons contribut the mobility of ions, such as the binding affinity to the fixed ion exchange sites, pH (affect the property of ion exchange membrane), specific ion channel. For example, if there is a ion with a strong the binding affinity to the membrane ion exchange sites, it will easier ion exchange the membrane and through the membrane under the electric field.

1.2. The main theory for anion exchange membranes with antifouling (reduced for organic fouling) property.

Colloidal fouling, organic fouling, scaling and bio-fouling are the main classification of ion exchange membrane fouling. Especially, the existent of large amount of organic fouling materials could easily coated on the AEMs surface, which increase the membrane electrical resistance tremendously in ED. Organic fouling on the AEMs surface mostly due to electrostatic and hydrophobic interactions. Therefore, the electrostatic forces of repulsion and hydrophilic materials modified on the AEM surface are the main methods to prepare the membrane with antifouling property, as shown in Figure S4 and Figure S5.

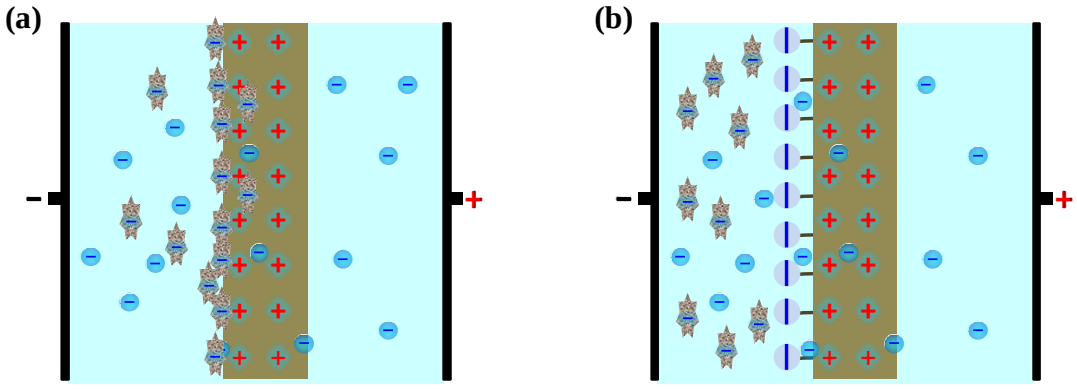

Organic fouling materials usually show the negative charge.

The electrostatic repulsion forces effect for antifouling.

Figure S4. The electrostatic forces of repulsion modified on the AEM surface for reduction of negatively charged original materials fouling in ED.

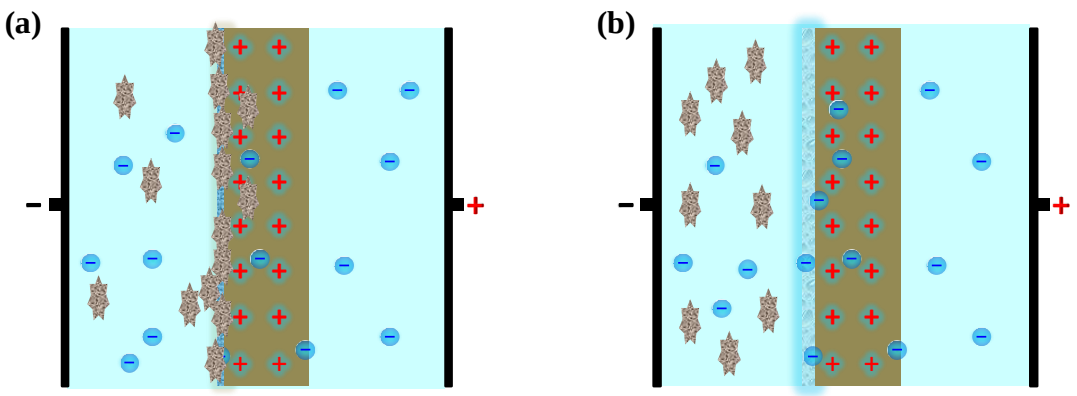

Figure S5. The hydrophilic materials modified on the AEM surface for reduction of hydrophobic original materials fouling in ED.

1.3. The theory for amide condensation reaction.

The large number of amino groups (-NH_2) in the 4-amino-benzenesulfonic acid monosodium salt (ABS) and poly(L-dopa) (L-PDA) with lots of carboxyl groups (-COOH), the amide condensation reaction was reacted between ABS and L-PDA under the catalyst of 1-ethyl-3-(3-dimethylami-nopropyl) carbodiimide hydrochloride (EDC-HCl) and N-hydroxy-succinimide (NHS), as shown in Figure S6.The amide condensation reaction is the negatively charged ABS were firmly grafted on the surface of L-PDA AEM by chemical bond (-NH-OC-).

Figure S6. The amide condensation reaction.

1.4. The theory of the L-dopa oxidized and self-polymerization

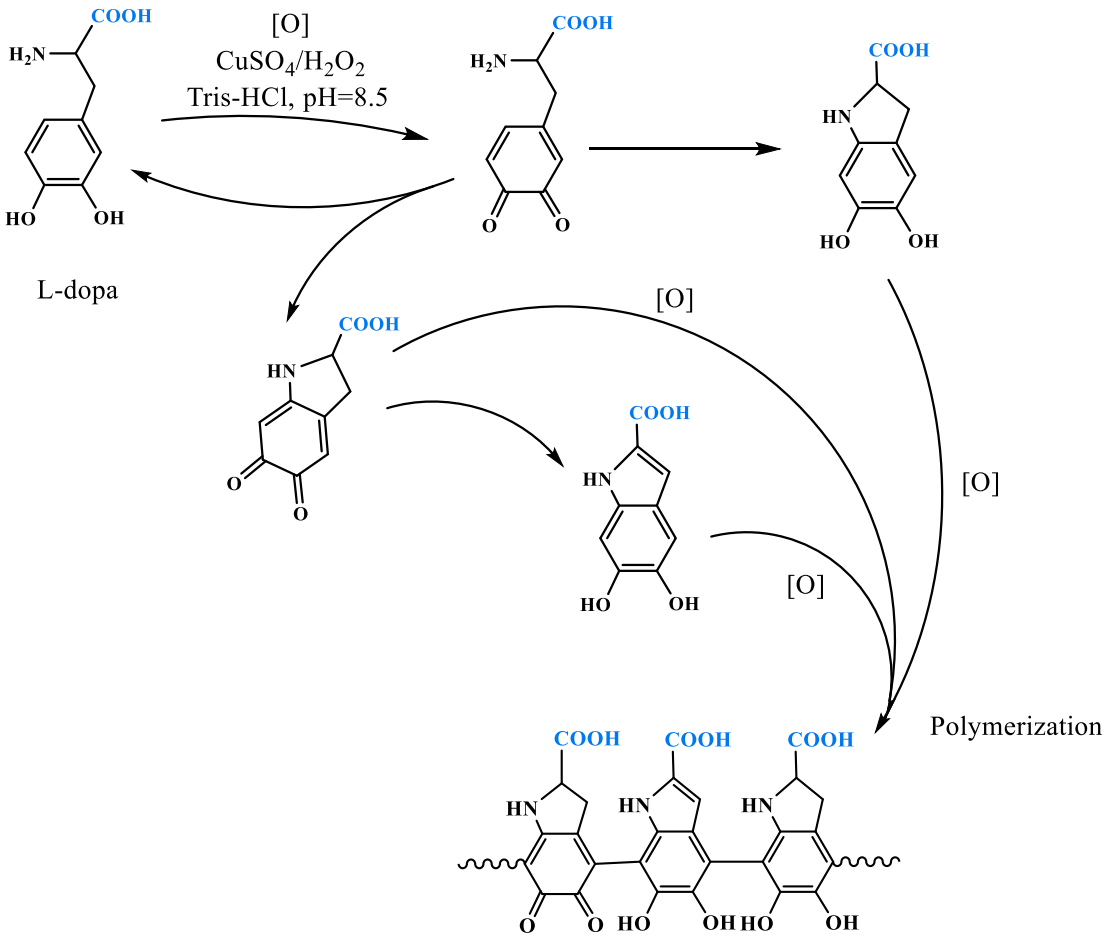

Figure S7. The theory of the L-dopa oxidized and self-polymerization

1.5. The concepts of Wenzel state for Young's model.

The mechanism of Wenzel state is a creative concept of "roughness factor" for the limitation of Young's model. In this concept, the actual contact area for a water droplet and the membrane surface is larger than the contact area of the apparent geometry. Due to the hydrophilic of the multilayer, it causes the surface more hydrophilic in geometry. In this theory, the variation of the surface hydrophilic is closed to the the roughness factor r and expressed by

$$r = \frac{\text{actual area on membrane surface}}{\text{apparent geometry area}}$$

the apparent contact angle $\cos\theta_a$ is calculated by

$$\cos\theta_a = \frac{r(\gamma^{mg}-\gamma^{mw})}{\gamma^{mw}}$$

According to this theory, once AEM surface covered with hydrophilic materials, the increasing of the surface roughness, the hydrophilic of membrane surface will increase.

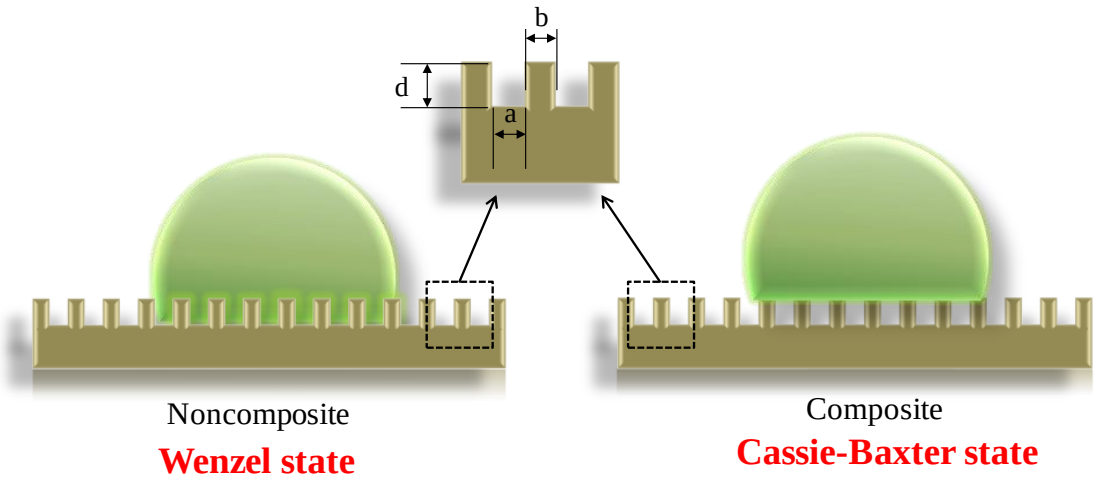

Figure S8. "Wenzel state" and "Cassie-Baxter state" for Young's model.

2. Methods

2.1. Fabrication of the monovalent anions selectivity layers of anion exchange membrane.

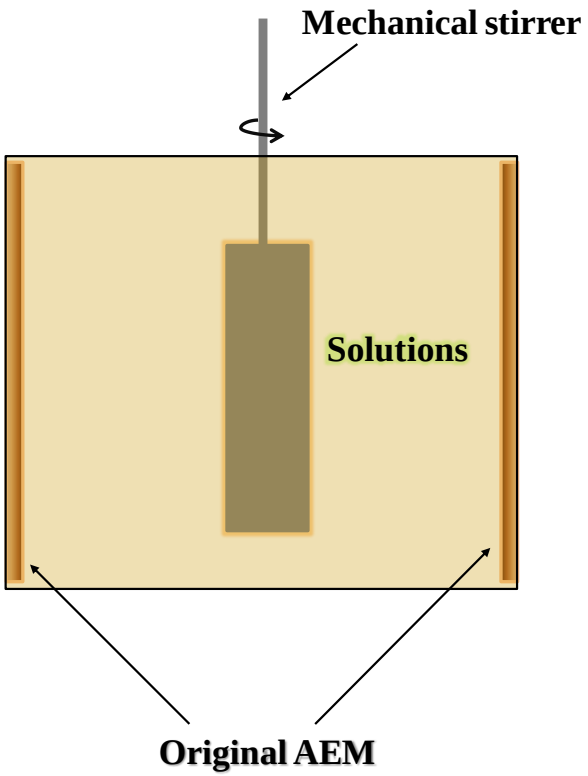

Figure S9. The scheme for preparation of monovalent anions selectivity layers of anion exchange membrane.

2.2. Preparation of the standard Tris-HCl, $CuSO_4/H_2O_2$ sholution

10 mM Tris-HCl were prepared and the solution should keep the pH = 8.8 by using 1 M HCl. Then, 5 mM Cu_2SO_4 was mixed into the solution. 1/750 (V/V) of H_2O_2 was mixed the solution and added in to the device immediately.

2.3. Scanning electronic microscopy (SEM)

The morphologies and structures of original AEM and L-PDA#ABS AEM (surface and cross-sectional) were characterized by using scanning electronic microscopy (SEM, Hitachi S-4800) at an accelerating voltage of 10.0 kV. The EDS maps C, O, N and S element over the membrane surface were provided at the same time.

2.4. Total reflectance Fourier transforms infrared (ATR-FTIR)

Total reflectance Fourier transform infrared spectroscopy (ATR-FTIR, Nicolet 6700, United States) was used to monitor the change of the functional groups between original AEM and L-PDA#ABS AEM surface. Membranes were dried thoroughly in vacuum oven at 60°C prior to measurements.

2.5. Atomic force microscopy (AFM)

Atomic force microscopy (AFM, Bruker, United States) equipped with a noncontact type scanner was used to acquire three dimensional topography of membrane surface. These images were captured under tapping mode at room temperature (~ 25°C). The root means square roughness (Rq), root average arithmetic roughness (Ra) and the mean difference between the highest peaks and lowest valleys (Rmax) were used to analyse the membrane surface roughness for a scanning area of 5 μm × 5 μm for each sample.

2.6. Measurement of surface electrical resistance and polarization current-voltage curve

In this work, for surface electrical resistance measurement, the constant current through the membrane is 0.004 A, and S is the membrane effective area, which is 7.065 cm^2.

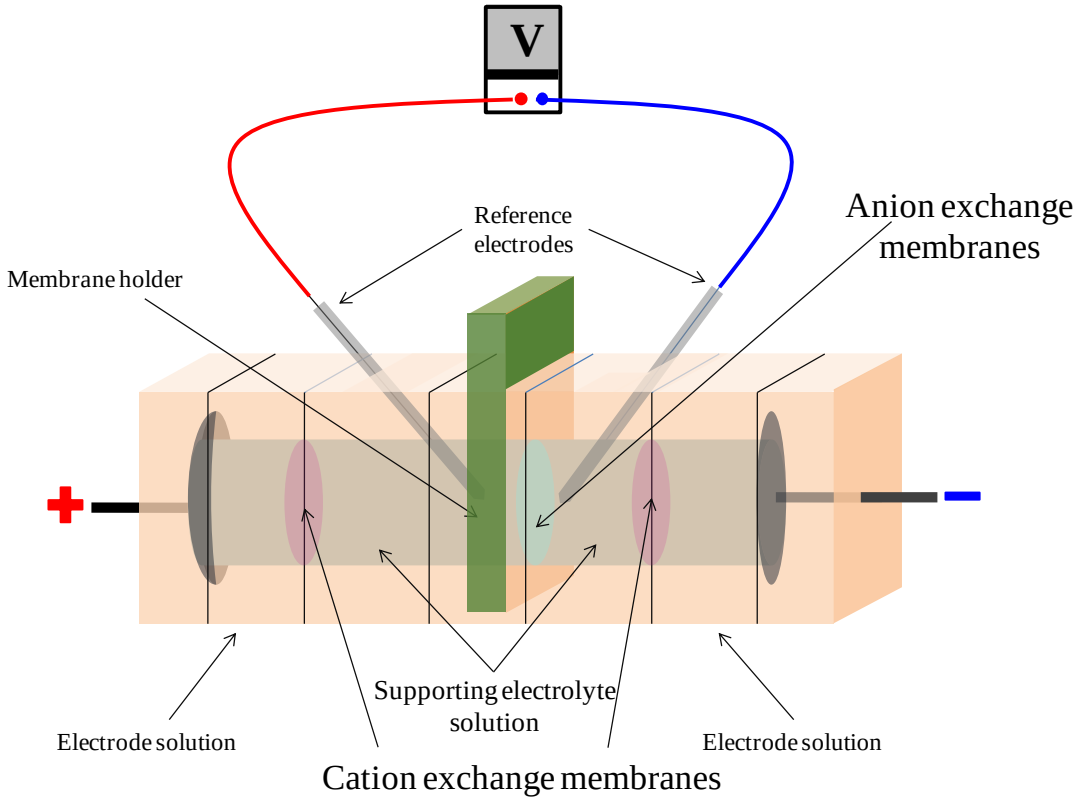

Figure S10. The membrane surface electric resistance measurement and polarization current-voltage curve device.

2.7. Measurement of the stability of fabricated layers.

5 hours in ED with reverse electrical field was chose to evaluate the stability of membrane modification layer (under the constant current and the current density was 10.0 $mA \cdot cm^{-2}$).

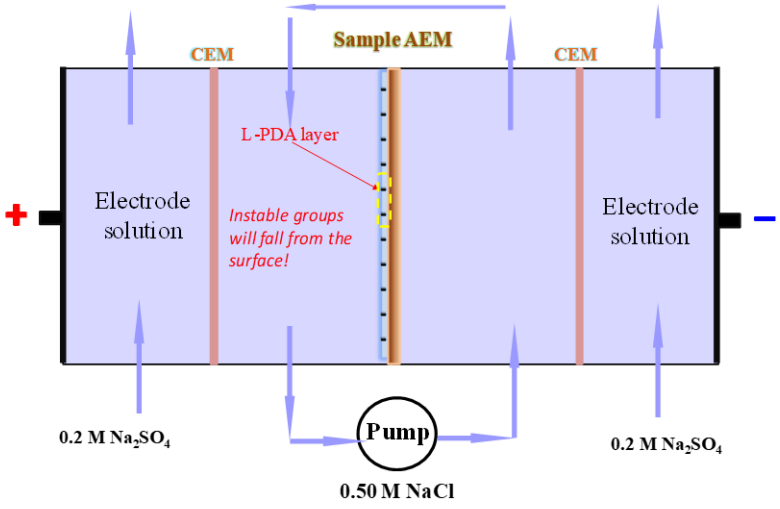

Figure S11. The scheme of lab-made electrodialysis device for membrane stability measurement.

2.8. Selective separation of monovalent anion measurement

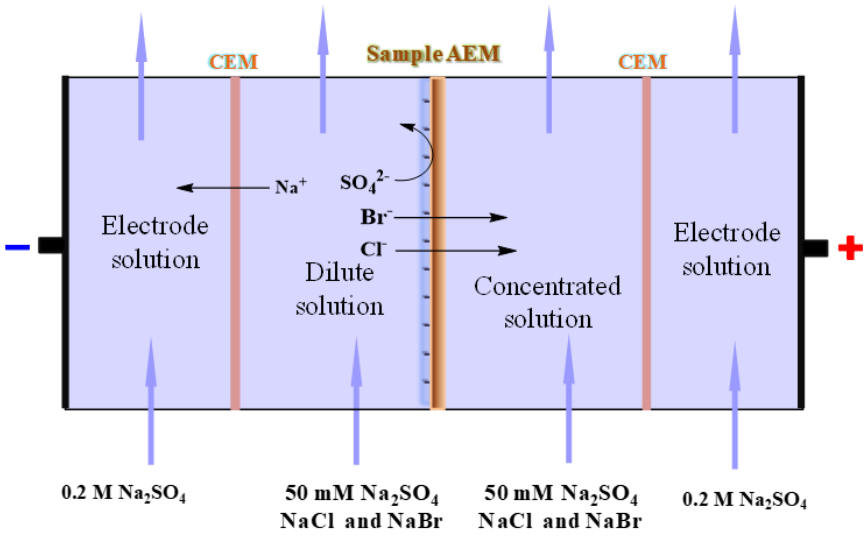

Figure S12. The scheme of lab-made electrodialysis device for selective separation of monovalent anions.

2.9. Antifouling property measurement

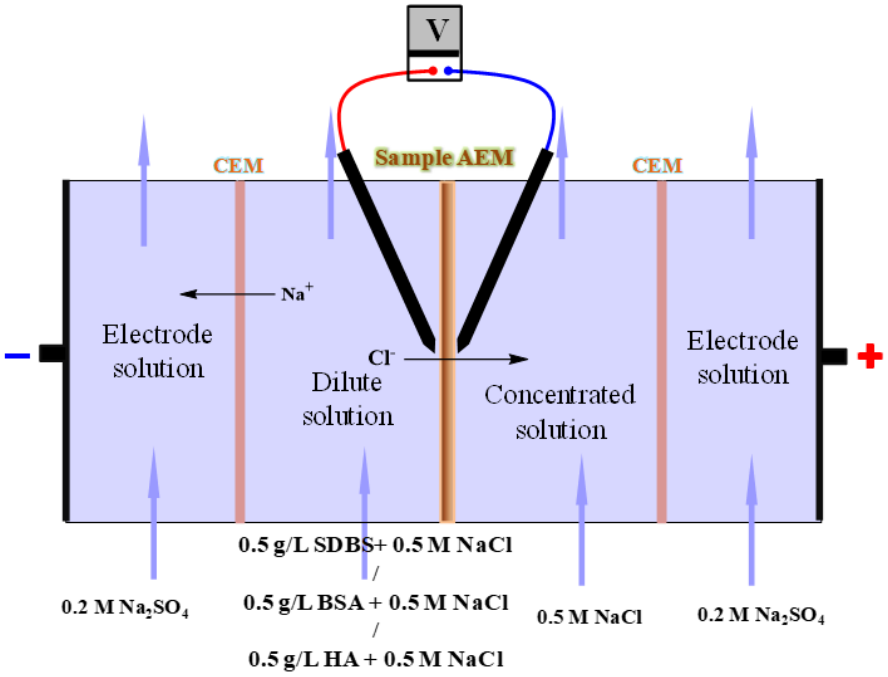

Figure S13. The scheme of the antifouling measurement.

3. Results.

3.1. The roughness and water contact angle of membranes

Table S1. The roughness and water contact angle of original AEM and L-PDA#ABS AEM.

Membranes type	Roughness/nm			water contact angle/°
	R_a	R_q	R_{max}	
Original AEM	5.68	7.38	39.5	105.2 ± 2.2
L-PDA#ABS AEM	7.02	8.59	49.5	68.6± 2.2

3.2. The equation of liner fit for the conductivity change of the original AEM, L-PDA AEM and L-PDA#ABS AEM in ED

$$\text{Equation: } y = a + b \cdot x$$

Table S2. The equation of liner fit for the conductivity change of the original AEM, L-PDA AEM and L-PDA#ABS AEM in ED.

Membrane type	Intercept (a)	Slope (b)
Original AEM	17.43356	-0.10222
L-PDA AEM	17.08994	-0.10263
L-PDA#ABS AEM	16.67853	-0.10748

3.3. The equation of liner fit for original AEM and L-PDA#ABS AEM in desalination.

$$\text{Equation: } y = a + b \cdot x$$

Table S3. The equation of liner fit for original AEM and L-PDA#ABS AEM in desalination of NaCl.

Membrane type	Intercept (a)	Slope (b)
Original AEM	5.84495	-0.07156
L-PDA#ABS AEM	5.81536	-0.07167

Table S4. The equation of liner fit for original AEM and L-PDA#ABS AEM in desalination of NaCl.

Membrane type	Intercept (a)	Slope (b)
Original AEM	5.79063	-0.06698
L-PDA#ABS AEM	5.71813	-0.06761

Table S5. The equation of liner fit for original AEM and L-PDA#ABS AEM in desalination of Na_2SO_4.

Membrane type	Intercept (a)	Slope (b)
Original AEM	9.38616	-0.05434
L-PDA#ABS AEM	9.46158	-0.05235

References

1. C. Zhang, Y. Ou, W. Lei, L. Wan, J. Ji, Z. Xu, *Angew. Chem. Int. Edit.*, 2016**, 55**, 3054-3057.
2. H. C. Yang, K. J. Liao, H. Huang, Q. Y. Wu, L. S. Wan, Z. K. Xu, *J. Mater. Chem. A*, 2014, **2**, 10225-10230.
3. S. Abdu, M. C. Marti-Calatayud, J. E. Wong, M. Garcia-Gabaldon, M. Wessling, *ACS Appl. Mater. Interfaces*, 2014, **6,** 1843-1854.
4. N. White, M. Misovich, A. Yaroshchuk, M. L. Bruening, *ACS Appl. Mater. Interfaces*, 2015, **7,** 6620-6628.
5. B. Van der Bruggen, A. Koninckx, C. Vandecasteele, *Water Res.* 2004, **38,** 1347-1353.
6. Y. Zhao, K. Tang, H. Liu, B. Van der Bruggen, A. Sotto Díaz, J. Shen, C. Gao, *J. Membrane Sci.*, 2016, **520,** 262-271.
7. Y. Zhao, J. Zhu, J. Ding, B. Van der Bruggen, J. Shen, C. Gao, *J. Membrane Sci.* 2018, **548,** 81-90.
8. Y. Zhao, C. Zhou, J. Wang, H. Liu, Y. Xu, J. W. Seo, J. Shen, C. Gao, B. Van der Bruggen, *J. Mater. Chem. A*, 2018, **6,** 18859-18864.
9. Y. He, L. Ge, Z. Ge, Z. Zhao, F. Sheng, X. Liu, X. Ge, Z. Yang, R. Fu, Z. Liu, L. Wu, T. Xu, *J. Membrane Sci.*, 2018, **563,** 320-325.
10. Y. Zhang, B. Van der Bruggen, L. Pinoy, B. Meesschaert, *J. Membrane Sci.*, 2009, **332,** 104-112.
12. Z. Xiong, T. Li, F. Liu, H. Lin, Y. Zhong, Q. Meng, Q. Fang, H. Sakil, W. Song, *Adv. Mater. Interfaces*, 2018, **5,** 1800183.
13. J. E, Y. Jin, Y. Deng, W. Zuo, X. Zhao, D. Han, Q. Peng, Z. Zhang, *Adv. Mater. Interfaces*, 2018, **5,** 1701052.
14. K. Boussu, B. Van der Bruggen, A. Volodin, J. Snauwaert, C. Van Haesendonck, C. Vandecasteele, *J. Colloid Interface Sci.*, 2005, **286,** 632-638.
15. J. Pan, J. Ding, R. Tan, G. Chen, Y. Zhao, C. Gao, B. Van der Bruggen, J. Shen, *J. Membrane Sci.*, 2017, **539,** 263-272.
16. H. Woehlk, J. Steinkoenig, C. Lang, L. Michalek, V. Trouillet, P. Krolla, A. S. Goldmann, L. Barner, J. P. Blinco, C. Barner-Kowollik, K. E. Fairfull-Smith, *Langmuir*, 2018, **34,** 3264-3274

17. Y. Jin, Y. Zhao, H. Liu, A. Sotto, C. Gao, J. Shen, *Sep. Purif. Technol.*, 2018, **207,** 116-123.
18. Y. Zhao, J. Zhu, J. Li, Z. Zhao, S. I. Charchalac Ochoa, J. Shen, C. Gao, B. Van der Bruggen, *ACS Appl. Mater. Interfaces*, 2018, **10,** 18426-18433.
19. B. J. Cardinale, *Nature*, 2011, **472,** 86-89.
20. B. Cohena, N. Lazarovitcha, J. Gilron, *Desalination*, 2018, **431,** 126-139.